XVI International Conference on Durability of Building Materials and Components
DBMC 2023, China
K.F. Li and D.P. Fang (Eds)

Damage Process Assessment of Mortar Samples under Freeze-thaw Cycles with Micro-CT and Expansion Measurements

Xi JI[1], Yuya Takahashi[1], Yuichiro Kawabata[2]

[1]Department of Civil Engineering, the University of Tokyo, Tokyo, Japan,
ji@concrete.t.u-tokyo.ac.jp (Xi JI), takahashi@concrete.t.u-tokyo.ac.jp (Yuya Takahashi)

[2]Port and Airport Research Institute, National Institute of Maritime, Port and Aviation Technology, Kanagawa, Japan, kawabata-y@p.mpat.go.jp (Yuichiro Kawabata)

Abstract. *The aim of this study is to comprehensively investigate the relationship between 3-dimensional crack development and mechanical degradation during Freeze-thaw cycles (FTC). An FTC test was designed in this study to relate the micro-scale crack patterns to the macro-scale expansion and mechanical property deterioration at different FTC damage levels. Mortar specimens with water-to-cement (w/c) ratios of 50% and 75% were cast in two sizes (i.e., Ø5×10 cm, Ø2×2.5 cm) and were subjected to FTCs. For Ø5×10 cm specimens, strain in the center part of the specimens were monitored by embedded mold gauges and compression tests were conducted at different expansion levels. For Ø2×2.5 cm specimens, X-ray micro computed tomography (micro-CT) and compression tests were conducted after different FTC durations. By comparing the test results of these two groups of specimens, the expansion, mechanical degradation, and development of micro-cracks in the mortar specimens during the FTC damage process were correlated. It is indicated that with similar mechanical reduction, the damage pattern differs in two w/c cases. This research provides a test method for investigating internal swelling damage and proposes the direction for further improvement of FTC simulation model.*

Keywords: *Freeze-thaw cycles, Multi-scale Damage, Micro-CT, Image Analysis.*

1 Introduction

Deterioration due to freeze–thaw cycle (FTC) is one of the most crucial causes of reduced durability in concrete structures. Many studies have focused on the mechanism and impact of FTCs (Sun and Scherer 2010, Sicat et al., 2013). However, the relationship between deterioration of mechanical properties and progression of FTCs tends to vary significantly across various FTC tests (Gong et al. 2022), which leads to difficulties in accurately modelling FTC deterioration in real structures. For deterioration induced by internal swelling mechanism, such as FTC and ASR, the damage patterns caused by the swelling products tend to be complex owing to distinct mechanisms. Therefore, obtaining the damage patterns of the microstructures during the deterioration process is crucial for a comprehensive understanding of the mechanical deterioration mechanisms. Many studies have investigated the damage evolution during FTC deterioration using either destructive or nondestructive test methods (Dong et al. 2018, Sokhansefat et al. 2020, Pilehvar et al. 2019). However, because the measurement of expansion or mechanical deterioration was not combined with that of the microstructural changes, the microscale damage and macroscale deterioration were not quantitatively related in these studies. The current study aims to investigate the simultaneous expansion, deterioration of mechanical properties, and microstructural damage progression throughout the entire FTC process and comprehensively understand the deterioration mechanism by relating these properties. To

achieve this, FTC tests were conducted on specimens of two different sizes. Image analysis was also conducted to quantify and visualize the interior damage of the mortar specimens at different FTC deterioration levels.

2 Experiments

2.1 Materials

Specimens of two sizes and two mix proportions were prepared, as listed in Table 1. The series name is denoted by size and water-to-cement ratio (w/c), for example, “s-50” denotes a small specimen (Ø 2×2.5 cm) with 50% w/c, “r-50” implies regular-size specimen (Ø 5×10 cm) with 50% w/c. “s-75-ct” and “s-50-ct” specifically denotes the specimen used for micro-focus X-ray computed tomography (micro-CT) test. Ordinary Portland cement with a density of 3.16 g/cm^3 was used for casting and an air-entraining agent (Master Air 202, BASF) was used to induce air. The fresh-air content was measured using the pressure method stipulated by ASTM C231.

The specimens were demolded one day after casting and cured in water at room temperature for 28 days. After water curing, the specimens were subjected to FTCs. The duration of each FTC was 240 min, with the maximum and minimum temperatures set to 10 °C and -20 °C, respectively. There were four stages in each FTC: cooling at -0.6 °C/min for 50 min, temperature holding at -20 °C for 70 min, heating at 0.6 °C/min for 50 min **,** and temperature holding at 10 °C for 70 min. This temperature setting was decided by trial tests to ensure that the center temperature of the specimen reached a minimum of -18±2 °C and maximum of 5± 2 °C during each cycle according to the temperature requirement for FTC test in JIS A 1148.

Table 1. Mix proportion and size of specimen series.

Specimen Series	Size (cm^3)	W/C	W (kg/m^3)	C (kg/m^3)	S (kg/m^3)	AE (C x %)	Fresh air content (%)
r-50	ø 5 × 10 cm	0.5	256	513	1376	0.012	8.3
s-50	ø 2 × 2.5 cm						
s-50-ct	ø 2 × 2.5 cm						
r-75	ø 5 × 10 cm	0.75	295	393	1376	0.02	7.7
s-75	ø 2 × 2.5 cm						
s-75-ct	ø 2 × 2.5 cm						

2.2 Methods

The tests conducted on the specimens in each series are presented in Table 2. For regular-sized specimens in ø 5 × 10cm (r-50, r-75), the continuous expansion development was recorded by the pre-embedded mold gauge at the center of the specimen (PMFL-60T-3TLJBT, Tokyo Measuring Instruments Lab). The specimens were removed from the FTC machine for the compression test when the expansion reached the target level, as listed in Table 2. The stress-strain relationships during the compression tests were recorded using a compressometer. For small specimens with a size of ø2 × 2.5 cm, compression test (s-50 and s-75) and micro-CT scanning (s-50-ct and s-75-ct) were conducted when the specimen went through certain FTCs, as stated in Table 2. Compression tests were conducted using a universal testing machine (Instron 34TM-50) with a 50 kN load cell. The micro-CT scanning was conducted with the CT scanner ScanXmate-D200RSS900, using a constant X-ray voltage of 180 kV and X-ray 80 μA

for each scan. After each scan and tomographic reconstruction, an image stack with dimensions of 1504 × 1504 × 1504 pixels was achieved. The resolution is 15.4 μm/pixel.

Table 2. Measurement and test for each series.

Specimen Series	Specimen Number	Timing of conducting test		
		Expansion measurement	Compression test	Micro-CT
r-50	12	throughout the entire FTC procedure	at expansion around 0, 150, 250, 400 μ	-
r-75	13	throughout the entire FTC procedure	at expansion around 0, 300, 500, 1500 μ	-
s-50	12	-	0, 60, 100, 200 FTC	-
s-75	12	-	0, 20, 40, 60 FTC	-
s-50-ct	3	-	-	0,60,100,200 FTC
s-75-ct	3	-	-	0,20,40,60 FTC

2.3 Image Segmentation

The micro-CT images were processed and segmented to extract damage patterns, which were then analyzed quantitatively. Preprocessing was conducted before segmentation to enhance the quality and reliability of the image analysis. First, a stripe filter was used to remove ring artifacts caused by the beam-hardening effect during scanning (Münch et al. 2009). To ensure an accurate comparison of the spatial changes in the microstructure of a specimen subjected to various FTCs, an elastic transformation was applied to the 3D image stack at each deterioration stage, aligning it to the reference image captured before the specimen was subjected to FTC. In addition, contrast enhancement, an unsharp mask, and a median filter were applied to the images to improve the edge enhancement and reduce noise. After preprocessing, segmentation was performed according to the grayscale and morphology. The Otsu threshold segmentation (Otsu 1979) was applied to separate the cracks, air voids, and background from the solid mortar. The waterflood-fill algorithm (Smith 1979) was then applied to filter the background. Subsequently, the spalling part at the current deterioration stage was obtained by extracting the deteriorated specimen from the specimen before FTC. In the next stage, morphological segmentation based on sphericity was performed to extract cracks from the crack-and-void phase. A combination of the segmented spalling and cracks was used to calculate the total damage volume of each scanned specimen at various deterioration stages.

3. Experimental Results

3.1 Specimens Sized ∅5 × 10 cm

3.1.1 Expansion

The expansion measured by the mold gauge embedded in the center of the ∅5 × 10 cm specimens is shown in Fig. 1. As mentioned earlier, each legend is a composite of the specimen

series and specimen number. For instance, the specimen labeled as “r-50-4” is the fourth specimen in the “r-50” series. Expansion data at the thawing temperature of 10 °C is extracted every 10 FTC. For both the 50% w/c and 75% w/c series, the expansion of the specimens was scattered with an increase in the FTC numbers. As shown in Figure 1(a), specimens with a 50% w/c exhibited notable resistance to FTC, possibly because of their low w/c and high air content. The expansion for r-50-11 and r-50-12 was only approximately 450 μ after a prolonged deterioration period of 800 FTCs. In contrast, Figure 1(b) shows that specimens with a 75% w/c ratio demonstrated low resistance to FTCs even with high air content, which yielded an expansion of 1500 μ after only 150 FTCs. This result is consistent with the common conclusions of FTC studies that higher w/c leads to lower resistance to FTC owing to increased porosity in the cement paste microstructures (Gong et al. 2017).

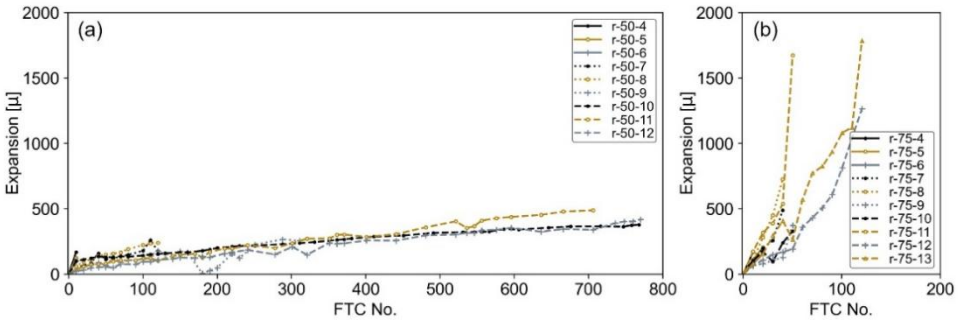

Figure 1 Expansion of (a) r-50 series, (b) r-75 series.

3.1.2 Compression test

Figures 2 and 3 show the stress-strain relationship during the compression test conducted on the specimens at different expansion levels for the r-50 and r-75 series, respectively. It is shown that the compressive strength increases slightly when the expansion is smaller than 200 μ, which might be caused by the hydration effect. The compressive strength in both series started to decrease with expansion growth when the expansion level went above 200 μ. To compare the relative reduction in the mechanical properties, the normalized strength and elastic modulus (relative to their initial values) are plotted in Figure 4. The deterioration of the mechanical properties in the r-50 series started from a much smaller expansion level than that in the r-75 series. When the relative compressive strength was reduced to 60% of the original value, the r-50 series exhibited an expansion level lower than 500 μ, while the r-75 series showed an expansion level of approximately 1500 μ.

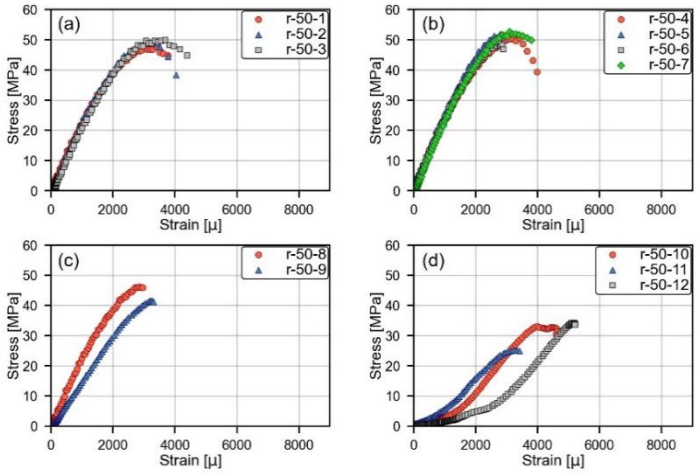

Figure 2 Compression behavior of r-50 series specimens at expansion levels of approximately (a) 0 μ (b) 150 μ (c) 250 μ, and (d) 400 μ.

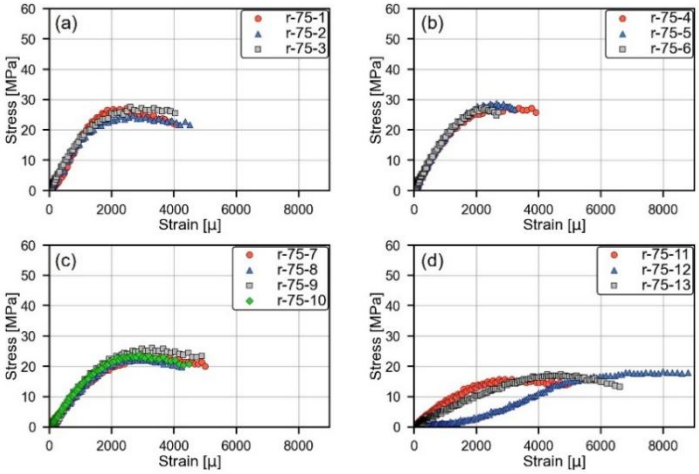

Figure 3 Compression behavior of r-75 series specimens at expansion levels of approximately (a) 0 μ (b) 300 μ (c) 500 μ, and (d) 1500 μ.

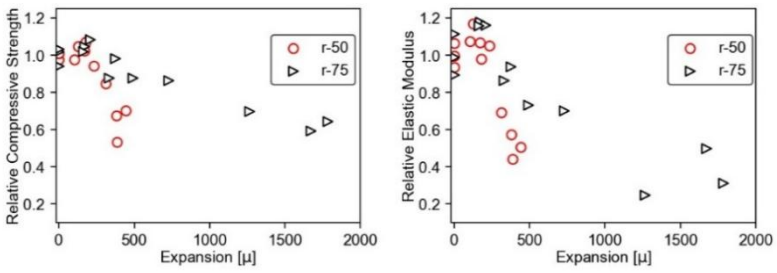

Figure 4 Relationship between expansion and (a) relative compressive strength, (b) relative elastic modulus

3.2 Specimens Sized $\emptyset 2 \times 2.5$ cm

3.2.1 Compression test

Compression tests and micro-CT scanning were conducted on specimen series s-50 and s-75 at various deterioration levels. Figure 5(a) illustrates the compressive strength of s-50 specimens at 0, 60, 100, 200 FTC, and Figure 5(b) illustrates the compressive strength of s-75 specimens at 0, 20, 40, 60 FTC. Figure 6 shows the relative compressive strength change process with an increase in FTC duration. Comparing the mechanical reduction ratios, specimens with a lower w/c reached the same deterioration levels slower. The relative compressive strengths of the s-50 series at 200 FTCs and the s-75 series at 60 FTCs were both approximately 0.6. The higher resistance of the lower w/c series shown in this test agrees with the conclusion of the expansion results explained in Section 3.1.1.

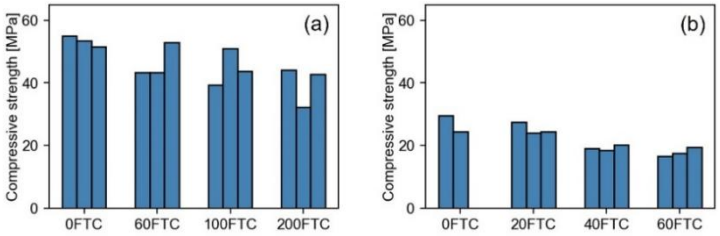

Figure 5 Compressive strength of specimens in (a) s-50, (b) s-75 series.

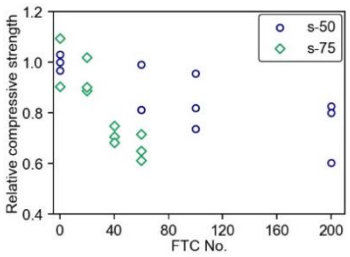

Figure 6 Relationship between relative compressive strength and FTC duration in s-50 and s-75.

3.2.2 Micro-CT scanning

Using the image analysis explained in Section 2.3, the damage to each scanned specimen at each FTC stage was segmented into cracks and spalling. Figures 7 and 8 show the 3D-reconstructed damage pattern changes of one specimen from series s-50-ct (s-50-ct1) and s-75-ct (s-75-ct1), respectively. For a clearer visualization, the segmented results of 400 slices were extracted for 3-D reconstruction, and damage patterns with a height of approximately 6 mm were reproduced. Figure 9 shows the damage proportion calculated from the segmented results of the three specimens in each series. It should be noted that the initial defects of the material, such as the wide interfacial transition zone (ITZ) is also identified as cracks due to displayed grayscale in images. For the 50% w/c series, the surface scaling proportion largely exceeded that of the cracks when a distinct damage increase was observed. In contrast, for the 75% w/c series, as the FTC progressed, both the proportion of cracks and spalling increased visibly during the FTC test.

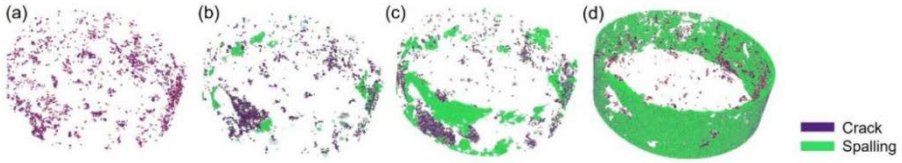

Figure 7 Reconstructed damage pattern of s-50-ct-1 after (a) 0 FTCs, (b) 60 FTCs, (c) 100 FTCs, and (d) 200 FTCs.

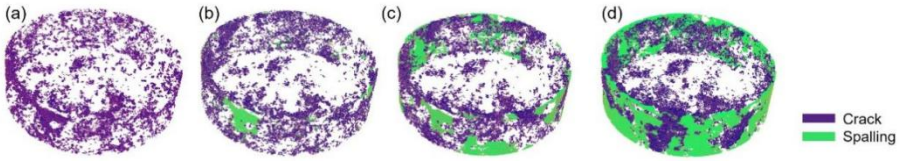

Figure 8 Reconstructed damage pattern of s-75-ct-1 after (a) 0 FTCs, (b) 20 FTCs, (c) 40 FTCs, and (d) 60 FTCs.

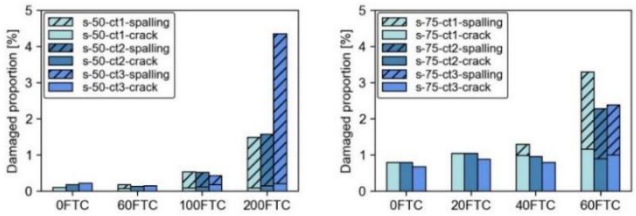

Figure 9 Damage proportion calculated from micro-CT images.

3.3 Discussion

Combining the results from the specimens of both sizes, it is evident that the damage to the 50% and 75% w/c specimens was caused by different mechanisms at similar mechanical deterioration stages. For the 75% w/c case, the fast increase of expansion in $\emptyset 5 \times 10$ cm specimens and the growth of crack volume in $\emptyset 2 \times 2.5$ cm specimens indicate that cracking caused by ice pressure plays a significant role in causing the mechanical deterioration in this high w/c group. As the FTC level increased, the ingress of water through the cracks led to the propagation of damage towards the interior of the specimen. In the serious deterioration stage, the damage was caused by both expansion and fatigue in the 75% w/c case. In contrast, in the 50% w/c case, cracking was almost negligible compared to the amount of surface scaling. This can be attributed to the low porosity of the specimen, which makes it difficult for water to penetrate the interior, resulting in minimal expansion. However, as the FTC duration increased, the fatigue induced by the cyclic ice pressure led to surface scaling, and the compressive strength of the specimens decreased accordingly.

4. Conclusion

In this study, a series of experiments were conducted to observe the simultaneous expansion increase, mechanical property deterioration, and microstructure damage development during the progression of FTCs. Using micro-CT scanning and image analysis, the different

deterioration mechanisms between the 50% and 75% w/c specimens could be better illustrated and understood. The conclusions of the experiments are as follows:

1. The expansion of the specimens with 50% w/c progressed slowly, but the compressive strength decreased when the FTC duration increased, even with a low expansion level. By contrast, the specimens with a w/c ratio of 75 % exhibited a higher expansion level with increasing FTC progress, leading to a corresponding decrease in the mechanical properties as the expansion continued.

2. The segmented damage patterns from the micro-CT scanning show that the damage of the 50% w/c specimens was composite by almost only surface scaling. In contrast, both the cracks and surface scaling continued to grow in the 75% w/c specimens. The image analysis results support the first conclusion that the mechanical property deterioration could be caused by both progression of ice-pressure-induced expansion and fatigue damage, which increased with the FTC duration.

3. Through the integration of mechanical and micro-CT testing, this study illustrates two different damage patterns resulting from two different mechanisms during FTC deterioration. Both mechanisms should be considered when modeling FTC deterioration in future studies.

Acknowledgement

This study was financially supported by JSPS KAKENHI 21H01416.

References

Dong, Y., Su, C., Qiao, P., & Sun, L. (2018). *Microstructural damage evolution and its effect on fracture behavior of concrete subjected to freeze-thaw cycles.* International Journal of Damage Mechanics, 27(8), 1272–1288.

Gong, F., Takahashi, Y., & Maekawa, K. (2017). *Strong Coupling of Freeze-Thaw Cycles and Alkali Silica Reaction—Multi-scale Poro-mechanical Approach to Concrete Damages.* Journal of Advanced Concrete Technology, 15(7), 346–367.

Gong, F., Zhi, D., Jia, J., Wang, Z., Ning, Y., Zhang, B., & Ueda, T. (2022). *Data-Based Statistical Analysis of Laboratory Experiments on Concrete Frost Damage and Its Implications on Service Life Prediction.* Materials, 15(18), 6282.

Münch, B., Trtik, P., Marone, F., & Stampanoni, M. (2009). *Stripe and ring artifact removal with combined wavelet—Fourier filtering.* Optics Express, 17(10), 8567. https://doi.org/10.1364/OE.17.008567

Otsu, N. (1979). *A threshold selection method from gray-level histograms.* IEEE Transactions on Systems, Man, and Cybernetics, 9(1), 62-66.

Pilehvar, S., Szczotok, A. M., Rodríguez, J. F., Valentini, L., Lanzón, M., Pamies, R., & Kjøniksen, A.-L. (2019). *Effect of freeze-thaw cycles on the mechanical behavior of geopolymer concrete and Portland cement concrete containing micro-encapsulated phase change materials.* Construction and Building Materials, 200, 94–103.

Sicat, E., Gong, F., Zhang, D., & Ueda, T. (2013). *Change of the Coefficient of Thermal Expansion of Mortar Due to Damage by Freeze Thaw Cycles.* Journal of Advanced Concrete Technology, 11(12), 333–346.

Smith, A. R. (1979). *Tint Fill*. In Proceedings of the 6th annual conference on Computer graphics and interactive techniques (pp. 276-283).

Sokhansefat, G., Moradian, M., Finnell, M., Behravan, A., Ley, M. T., Lucero, C., & Weiss, J. (2020). *Using X-ray computed tomography to investigate mortar subjected to freeze-thaw cycles.* Cement and Concrete Composites, 108, 103520.

Sun, Z., & Scherer, G. W. (2010). *Effect of air voids on salt scaling and internal freezing.* Cement and Concrete Research, 11.